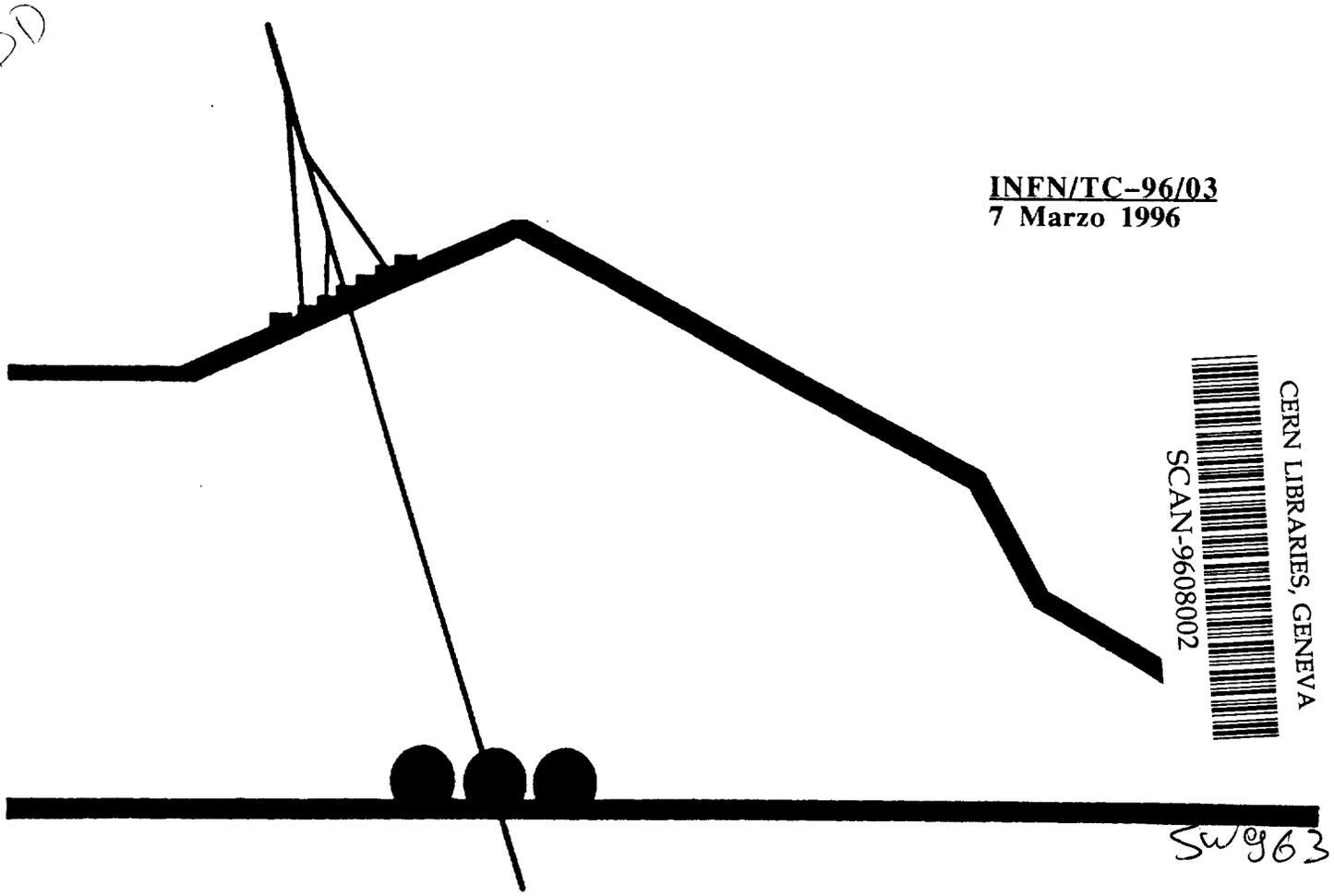

INFN/TC-96/03
7 Marzo 1996

Performance and Simulation of Glass Spark Counter

G. Bencivenni, M. De Deo, M. D'Incecco, G. Felici, C. Gustavino

*(contrib. to "RPC95", Pavia, October 11-12, 1995
the 3rd Int. Workshop on Resistive Plate Chambers
and Related Detectors)*

INFN - Laboratori Nazionali del Gran Sasso

Published by **SIS–Pubblicazioni**
dei Laboratori Nazionali di Frascati

INFN - Istituto Nazionale di Fisica Nucleare
Laboratori Nazionali del Gran Sasso

INFN/TC-96/03
7 Marzo 1996

PERFORMANCE AND SIMULATION OF GLASS SPARK COUNTER

M. De Deo[1], M. D'incecco[1], C. Gustavino[1], G. Bencivenni[2], G. Felici[2]

Abstract

In this paper the modular Glass Spark Counter is described. The detector performance as a function of the construction parameters is also discussed, making use of a simulation where the detector is treated as an electronic network.

INTRODUCTION

Besides the different design, the main difference between the modular Glass Spark Counter (GSC) and the standard RPC is the use of glass instead of bakelite as electrode material.

The advantage of glass is due to its homogeneity and to the excellent surface quality of this material; these allow the realization of noiseless devices without any surface treatment. Another advantage of glass is its stability with the detector operation, while with some other materials (i.e. bakelite, ABS), the resistivity increases with time due to their ionic conductivity. If the GSC is operated in the saturated mode, the inexpensive float glass ($\rho \sim 10^{12}\Omega$cm) is adequate for low rate applications, while the iron-oxide doped glass ($\rho \sim 10^{10}\Omega$cm) is suitable for particle rates up to about 100 particles/cm^2/s [1].

The good results obtained with the modular GSC prototypes, in terms of reliability and performance, encouraged us to start an R&D program to develope optimized new detectors in a fully engineered way.

In this paper we describe the present GSCs and we discuss the detector performance as a function of the detector parameters by means of a detector simulation.

[1] INFN–Laboratori Nazionali del Gran Sasso, ss 17 bis Km 18+910, I–67010 Assergi L'Aquila
[2] INFN –Laboratori Nazionali di Frascati, P.O. Box 13, I 00044–Frascati (Roma) Italy

STRUCTURE OF THE DEVICE

A sketch of the modular GSC is shown in fig.1. It consists of a pair of glass electrodes 2 m long, 8 cm wide and 2 mm thick. The 2 mm distance between the electrodes is ensured by precision Delrin spacers which clamp the edges of the plates. These "E" shaped spacers sustain both the electrodes, ensuring a gap tolerance at the level of a few microns. The high voltage is applied to the electrodes by means of a coating of water-based graphite, with a surface resistivity of about 200 kΩ/square. The gas containment is ensured by a PVC envelope which is the same used in the standard streamer tubes. The extrusion of opportune envelopes will permit the realization of larger detectors. The H.V. connections to the graphite are located in one of the two end caps that close the GSC module. External pick-up electrodes (not shown in fig.1) are used to detect the induced pulses. All the materials used are commercially available, while the needed manpower is essentially due to the graphite coating and to the assembly. An estimate for large scale production is of the order of \$100/m^2 [2].

PERFORMANCE

A set of measurements has been performed with a telescope made up of 4 horizontal planes 20 cm apart; each of them is realized with 12 GSCs 1 m long and equipped with orthogonal X and Y pick-up strips 3 cm wide. Fig.2 shows the display of a muon event.

Fig.3 shows the single counting rate of a plane as a function of the high voltage. The gas mixture is Ar + IsoC_4H_{10} + Freon 13B1 = 60% + 35% + 5%. A wide plateau is visible, the counting level being essentially due to the cosmic rays and to the ambient radioactivity.

The plane efficiency as a function of the high voltage is shown in fig.4. This measurement has been done selecting the muon events with a track around the vertical direction in both X and Y views. The 92% efficiency level is due to the geometrical dead area, the measured intrinsic device efficiency being more than 99%. The plane efficiency can be increased by about 3% by improving the contruction of the 8 cm wide GSCs. The contruction of 25 cm wide detectors is foreseen to obtain a 98% plane efficiency.

Cosmic ray muons, selected by using a scintillator telescope and a lead absorber 10 cm thick, have been used to measure the time resolution of GSCs. A fast scintillator, with a r.m.s. time resolution of about 150 ps has been used as reference detector. The time distribution of one GSC with respect to the reference scintillator is shown in fig.5. The supplied voltage is 8.6 kV; the measuring time is about 32 days. The distribution is fitted with 2 gaussians. The main one has a standard deviation of about 480 ps. The tail of the distribution is due to sparks that develope where

the electric field is lower than the nominal value. This tail can be strongly reduced by recording the first signal coming from 2 stacked detectors, as they are crossed by the same particle. Fig.6 shows the time distribution obtained by using 2 GSCs. For this configuration the resulting distribution is more symmetrical and the standard deviation of the fit is improved to 390 ps.

As for streamer tube based calorimeters, the energy measurement of a shower can be performed either by the digital hit counting of the fired pick-up or by measuring the total charge, that is proportional to the total number of streamers and thus to the shower energy. At low energy, the digital read-out gives better results than the total charge measurement. In fact, the digital read-out is almost independent of the single streamer charge fluctuaction. At high energy (more precisely at high track densities) the analog read-out is preferable to avoid saturation effects due to the non-negligible probability of having more than one track under the same pick-up.

For low energy e.m. showers, the digital read out gives good results also with the GSCs [4]. To assess the possibilities for using the GSC as a basic device in charge measuring sampling calorimeters, we have measured the charge response for vertical cosmic ray muons. Fig.7 shows the charge spectrum using a 120 ns integration time. The large time window used includes most of the afterpulses produced following the main spark, so that a secondary peak and a slightly long tail is visible in the spectrum. By using a 30 ns gate the afterpulses are cut off and the tail is strongly reduced (fig.8). The FWHM/peak of the distribution is about 20%, with very little high charge tail; only 12% of the pulses gives charge greater then 1.5 times the peak charge. As a comparison, the distribution for streamer tubes has a FWHM/peak of about 55%, with 15 - 20% of the pulses giving a charge 1.5 times the peak charge [5].

SIMULATION

To study the performance as a function of the detector parameters, we have carried out a detector simulation based on the SPICE program [6]. In this simulation, the GSC is treated as a lattice of proper resistors and capacitors. The spark is simulated with a short circuit between the electrodes, through a time variable resistor.

The essential input parameters are:

-Gap value;

-Electrode thickness,resistivity and dielectric constant;

-Graphite resistivity;

-Distance between the pick-up planes and the electrodes.

-Strip width.

-Lattice size and granularity.

In the following, if not otherwise specified, we will use these default parameters: gap=2 mm; electrode thickness=2 mm; $\rho = 10^{12}\Omega$cm; ϵ_r=5; σ=200 kΩ/square; distance between the pick-up planes and the electrodes=2 mm; strip width=10 mm.

A first result of the simulation is the confirmation of the well-known dependence of the induced charge with the pick-up plane distances respect to the electrodes. A uniform distance is essential to obtain a narrow distribution like the one shown in fig.8. In the case of a digital read-out, a disuniformity can give rise to inefficiency and/or high multiplicity problems. Fig.9a shows the signal on the strip facing the spark location (central strip); fig.9b shows the side strip signal, that is, the signal from the strip neighbouring the central one. Fig.10 shows the pulses in the real detector (the pulse signs are opposite to that of the simulation because the signals come from the strips faced to the anode, while in the simulation the signals are calculated for the strips close to the cathode). The central/side strip peak amplitude obtained with the simulation is about 3, in agreement with the measured one. The distortion of the induced pulses is due to the graphite resistivity value. Referring to fig.9a, the signal from the central strip has an exponential negative tail after the positive pulse. In fact, the current due to the spark charges up the graphite-strip capacitance, giving a positive pulse. The capacitance discharges through the graphite in a time proportional to its resistivity, giving the exponential tail. On the side strip (fig.9b), the pulse shape is qualitatively different: the tail following the initial pulse starts positive before eventually going negative. In this case, the positive tail is due to the extra charge coming from the discharge of the central strip through the graphite. Therefore, a charge measurement is very sensitive to the graphite resistivity and depends on the integration time. In fig.11, the central/side strip integrated charge ratio is plotted as a function of the integration time window for 3 different resitivity values. We note that large integration times give rise to a broadening of the charge distribution on the strips even at relatively high resistivity values.

Fig.12 shows the electrode transparency as a function of the graphite resistivity. As a definition of the electrode transparency, the ratio between the central and the side strip peak amplitude, normalized to the limit for very high resistivity, is assumed. The simulation result is in good agreement with the experimental data, as shown in fig.12. For resistivities higher than a few hundred kΩ, a full transparency can be achieved.

Finally, the pulse rise time weakly depends on the detector parameters. In practice, the crucial parameter to obtain a good time resolution is the gap uniformity, which must be at least a few tens of microns to achieve a time resolution of one nanosecond.

CONCLUSION

The modular GSC is a noiseless detector with a time resolution of a few hundred picoseconds and interesting charge properties. Its design and the materials used permit a large production at low cost. The detector simulation will be used to contruct new detectors, to optimize detector parameters.

REFERENCES

[1] G.Bencivenni et al., Nucl. Instr.& Meth. A 332 (1993) 368-372.
[2] M.Meoni (POL.HI.TECH), private communication.
[3] M.G.Catanesi et al., Nucl. Instr.& Meth. A 247 (1986) 438-444.
[4] G.Bencivenni et al., Nucl. Instr.& Meth. A 315 (1992) 507-512.
[5] E.Iarocci, Nucl. Instr.& Meth. 217 (1983) 30-42.
[6] SPICE, E. Cohen, D.O. Pederson University of California, College of Engineerings, Dept. of Electrical Engineering and Computer Science.

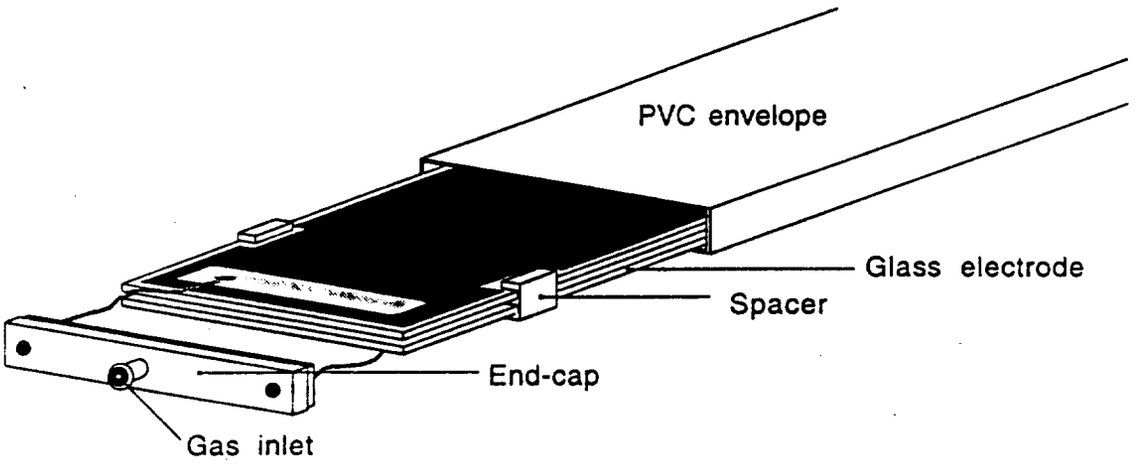

Fig. 1. Sketch of a GSC module.

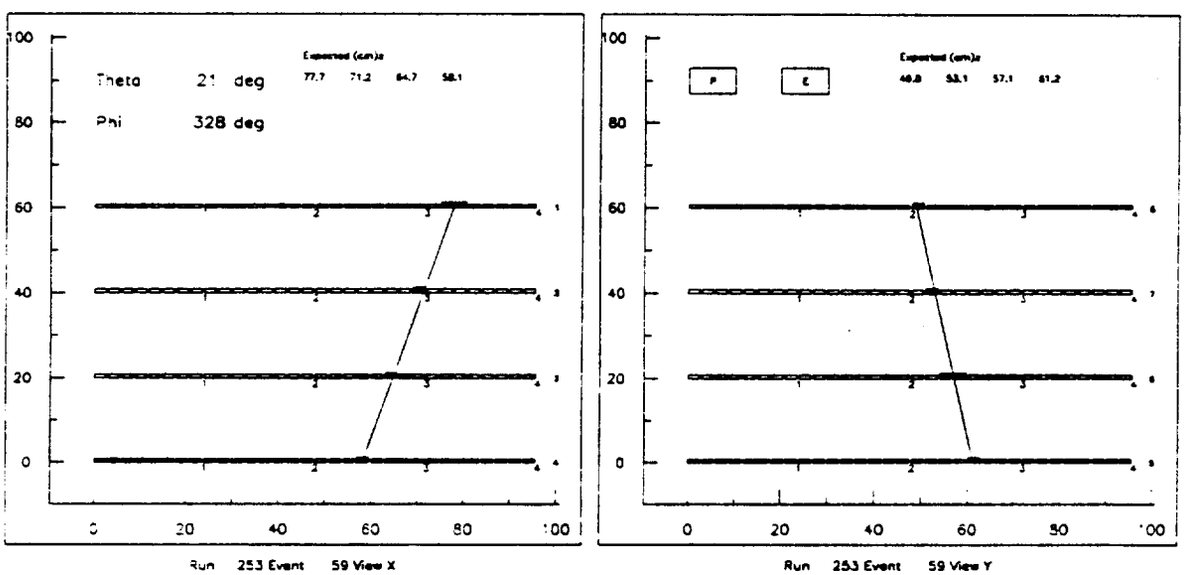

Fig. 2. Display of a muon event (X and Y views).

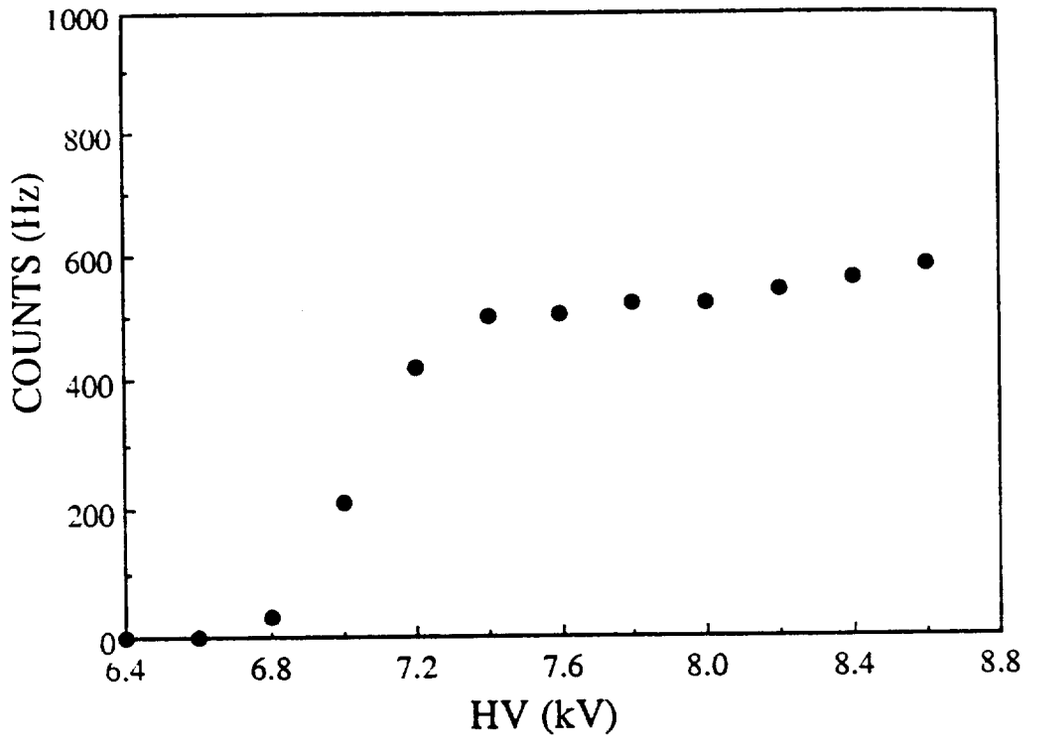

Fig. 3. Single counting rate as a function of the high voltage for a 1 m^2 GSC plane.

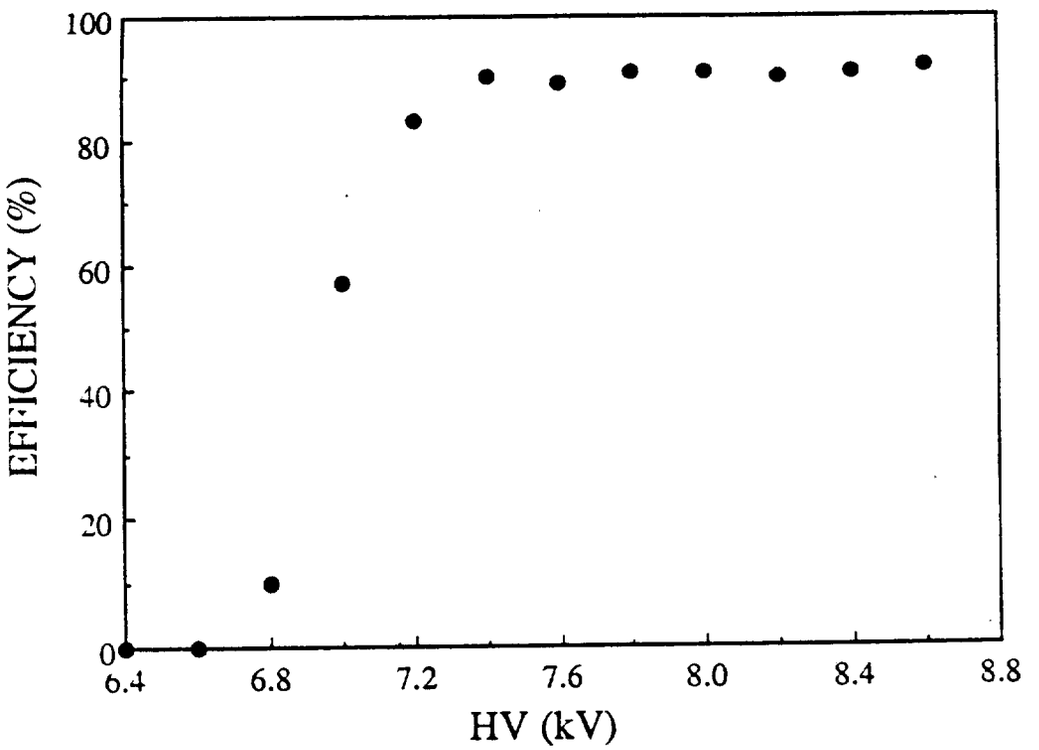

Fig. 4. Detection efficiency as a function of the high voltage for a 1 m^2 GSC plane.

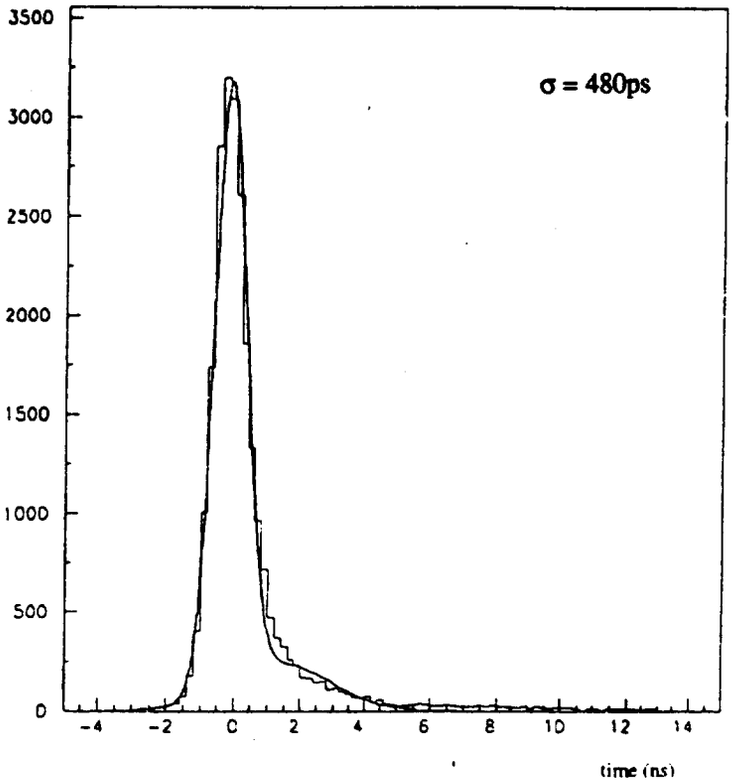

Fig. 5. Time distribution of one GSC with respect to a fast scintillator.

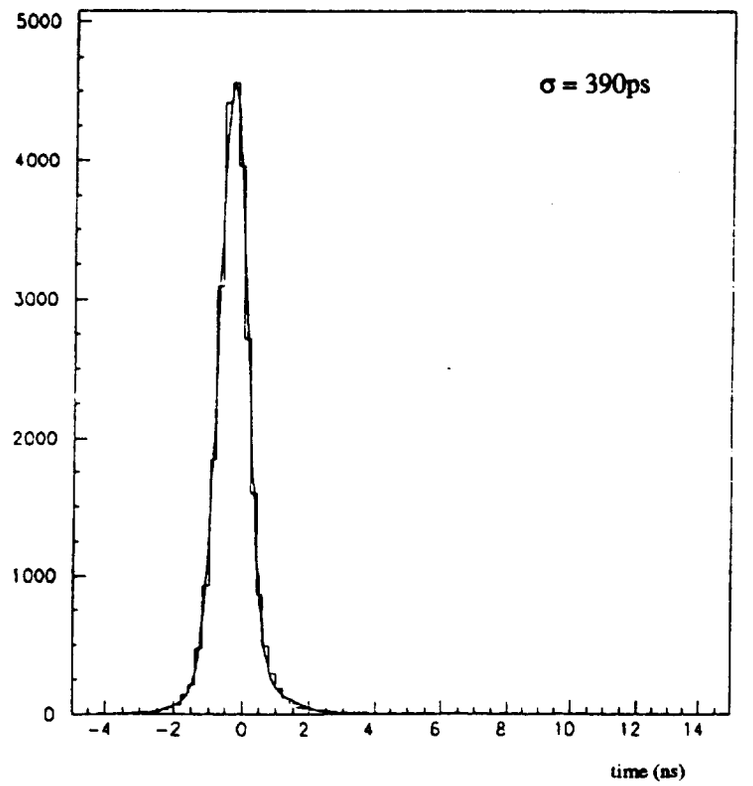

Fig. 6. Time distribution of 2 stacked GSCs with respect to a fast scintillator.

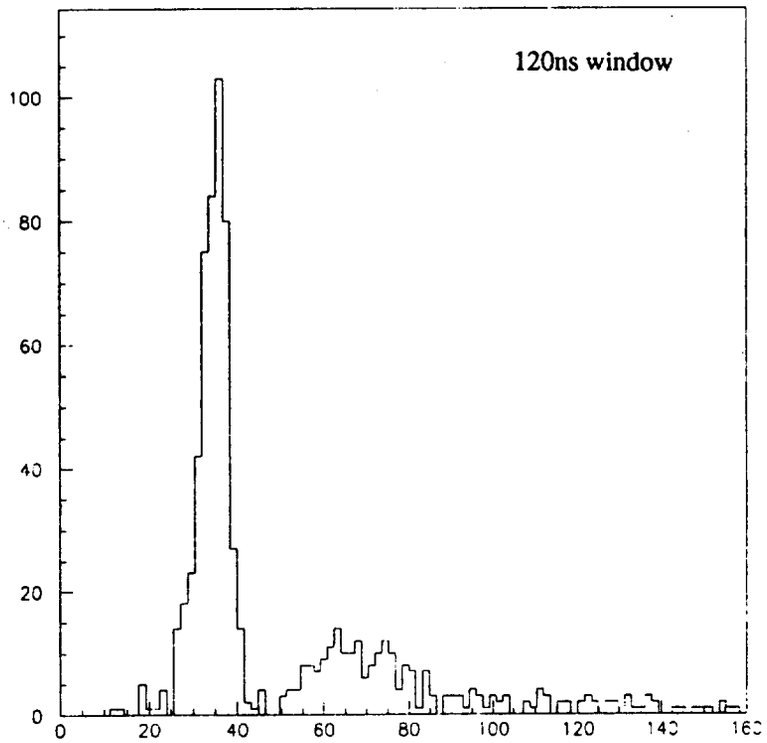

Fig. 7. Charge spectrum of a GSC (H.V.=7.4 kV, 120 ns gate).

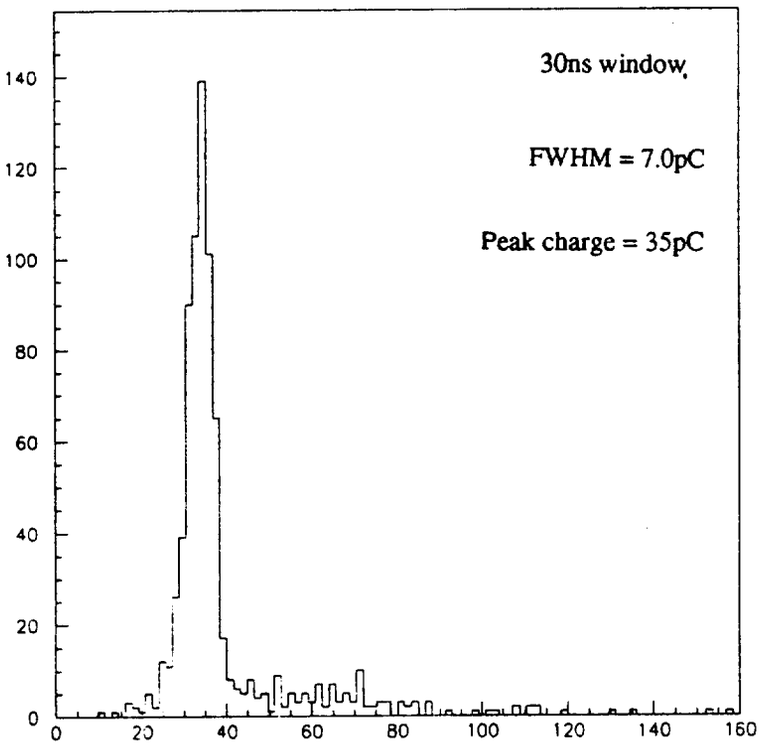

Fig. 8. Charge spectrum of a GSC (H.V.=7.4 kV, 30 ns gate).

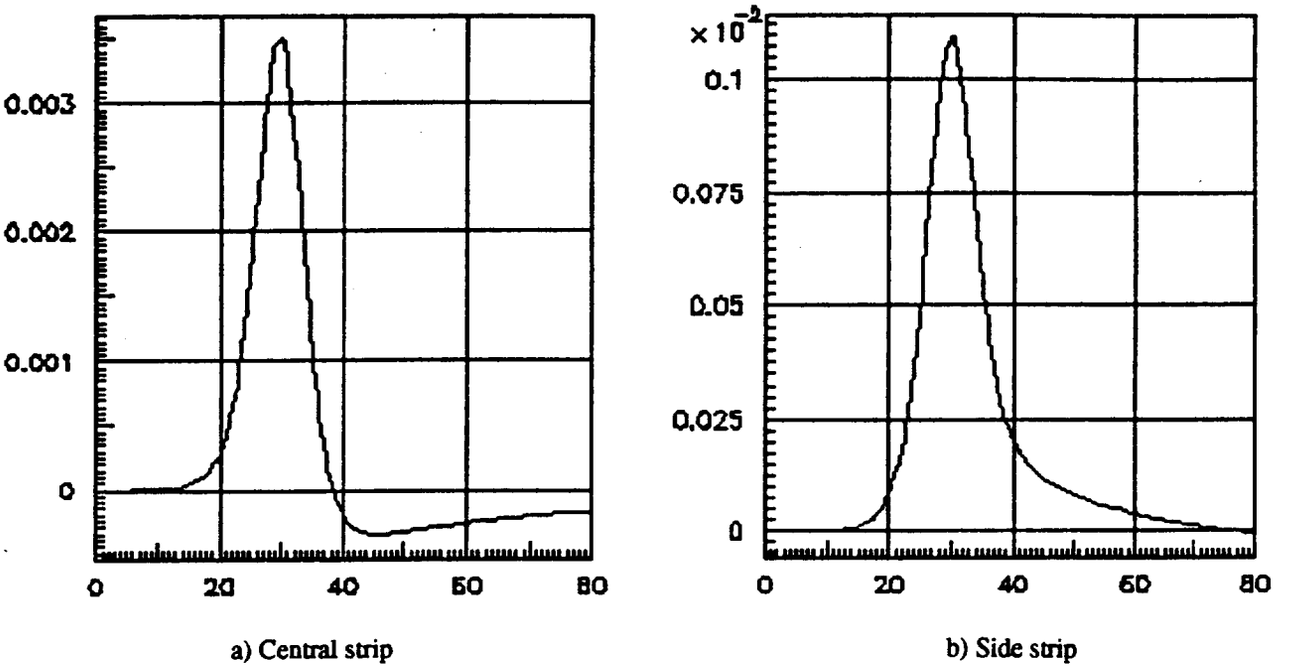

Fig. 9. Simulated pulses on 1 cm wide strips. a) Central strip; b) side strip.

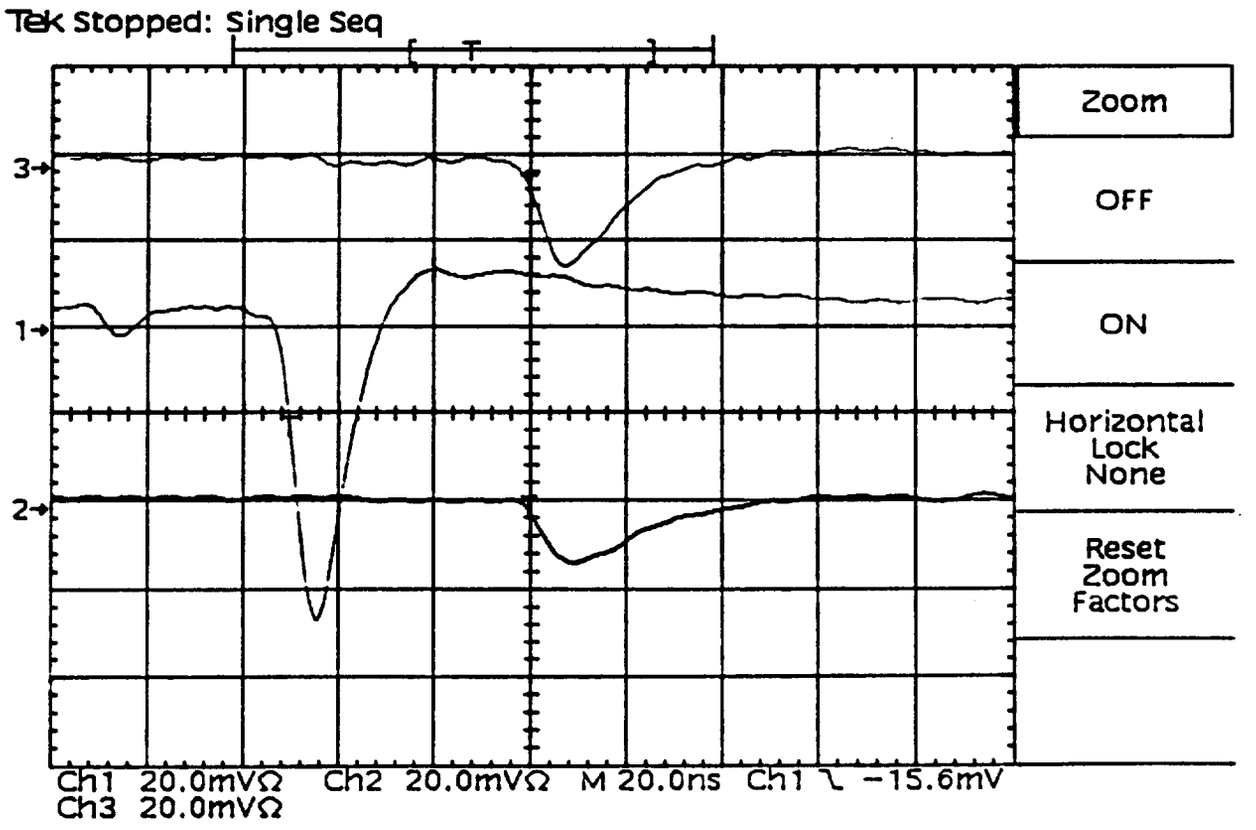

Fig. 10. Induced pulse on strips in the modular GSC. Ch.1: Central strip; Ch.2,3: side strips. 50 Ω load.

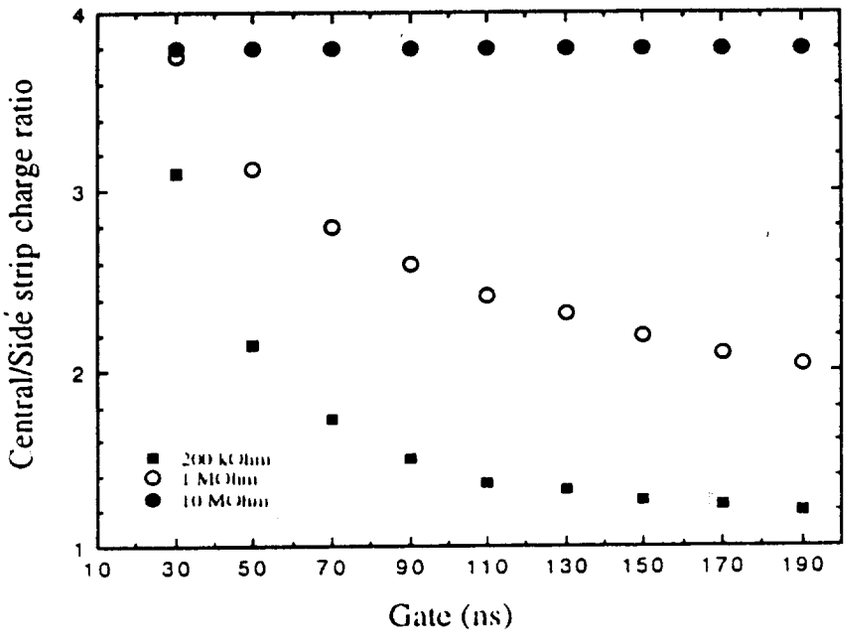

Fig. 11. Central/side strip integrated charge ratio as a function of the integration time windows, for σ = 200 kΩ/square, σ = 1 MΩ/square, σ = 10 MΩ/square.

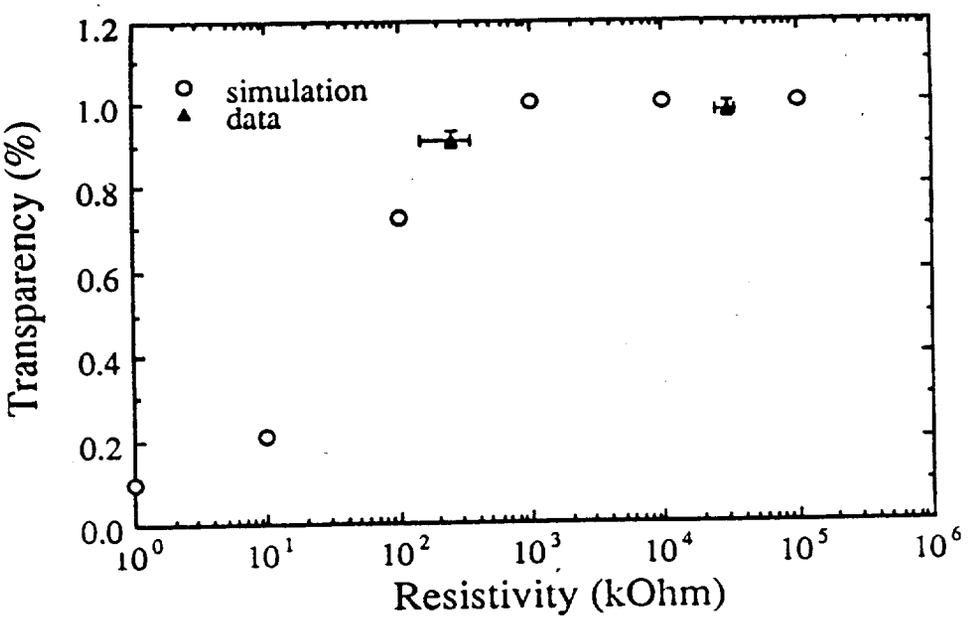

Fig. 12. Cathode transparency as a function of the graphite resistivity.